Miniaturization effect of electroosmotic self-propulsive microswimmer powered by biofuel cell

Toshiro Yamanaka[*] and Fumihito Arai

Abstract

For future medical microrobotics, we have proposed the concept of the electroosmotic self-propulsive microswimmer powered by biofuel cell. According to the derived theoretical model, its self-propulsion velocity is inversely proportional to the length of the microswimmer, while it is proportional to the open circuit potential generated by the biofuel cell which does not depend on its size. Therefore, under conditions where those mechanisms work, it can be expected that the smaller its microswimmer size, the faster its self-propulsion velocity. Because of its remarkable feature, this concept is considered to be suitable as propulsion mechanisms for future medical microrobots to move inside the human body through the vascular system, including capillaries. We have already proved the mechanisms by observing the several 10 μm/s velocity of 100 μm prototypes fabricated by the optical photolithography using several photomasks and alignment steps. However, the standard photolithography was not suitable for further miniaturization of prototypes due to its insufficient resolution. In this research, we adopted femtosecond-laser 3D microlithography for multi-materials composing of the conductive polymer composites and nonconductive polymer composite and succeeded in fabricating 10 μm prototypes. Then we demonstrated more than 100 μm/s velocity of the prototype experimentally and proved its validity of the smaller and faster feature.

Keywords: Micro/nano robots, Microswimmer, Glucose biofuel cell, Electroosmotic flow, Conductive/nonconductive polymer composites, Two photon polymerization

Introduction

Biomedical swimming microrobots have great potential for use in innovative medicine, such as long-term drug delivery and painless pinpoint surgery. It has been discussed that microrobots autonomously explore the human body through the vascular system and carry out various medical tasks [1]. To achieve this, propulsion and energy supply in microscale biological fluids are the most significant challenges. These developments will require utilizing what can be supplied in the human body as energy sources and applying a propulsion principle that can operate effectively at the microscale. Furthermore, robots capable of swimming against the flow in capillaries are desirable because they can approach most tiny spaces in the body and perform various tasks such as attacking tumors. More specifically, we require mechanisms to realize robots with their size less than a few 10 μm which can swim with velocities more than a few 100 μm/s comparable to capillary flow velocity [1]. A number of microscale propulsion mechanisms have been reported such as external-fields-powered propulsions [2–5], microorganism-powered propulsions [6], and catalytic self-propulsions [7–10] by bubbles and/or phoretic flows. However, no mechanism has yet been established to meet the above requirements.

Considering those requirements, we have proposed the concept of the self-propelled microswimmer using electroosmotic propulsion (EOP) and biofuel cell (BFC) [11].

*Correspondence: yamanaka@biorobotics.mech.nagoya-u.ac.jp
Department of Micro/Nano-Mechanical Science and Engineering, Nagoya University, Furo-cho, Chikusa-ku, Nagoya 464-0814, Japan

The BFC mechanism generates an open-circuit potential (OCP) by decomposing biofuels that are present in the human body, such as glucose and oxygen. The EOP mechanism creates self-propulsion velocity by a reaction force of electroosmotic flow (EOF), with the OCP as the energy source. According to the derived theoretical EOP model, its self-propulsion velocity is inversely proportional to the length of the microswimmer, while it is proportional to the OCP which does not depend on its size. Therefore, under conditions where both BFC and EOP mechanisms work, it can be expected that the smaller its microswimmer size, the faster its self-propulsion velocity. This remarkable feature can make this concept the best solution to those requirements. We proved the concept by observing the self-propulsions of 100 μm prototypes with several 10 μm/s velocity in a glucose solution. The prototype consisted of one insulating layer made of UV-curable polymer SU-8 and two conductive polymer composite layers consisting of SU-8 and silver (Ag) nanoparticles (NPs) on which specific enzymes were immobilized and was fabricated by the optical photolithography using several photomasks and alignment steps. However, the standard photolithography was not suitable for further miniaturization of prototypes due to its insufficient resolution.

In this paper, we report new smaller prototypes capable of swimming with faster velocities in a glucose solution. We adopted the fabrication method suitable for them using femtosecond-laser 3D microlithography [12] and multi-materials composing of the conductive polymer composites (CPCs) and nonconductive polymer composite (NCPC). Then we evaluated the self-propulsion velocity of the prototypes experimentally to prove its validity of the smaller and faster feature.

Materials and methods
Concept and physical model
Figure 1a shows the concept. The BFC comprises a redox-electrode pair, with through-holes for drainage. One electrode works as a bioanode oxidizing glucose, and the other as a biocathode reducing oxygen. The BFC mechanism generates an OCP between the electrodes by the redox reactions. The EOP mechanism comprises an electrically insulating tube arranged between them. Electric force by the OCP generates a plug flow of electrolyte within the tube (i.e., EOF). Its reaction force then drives the tube in the opposite direction to the EOF. Due to the EOF characteristics, this EOP mechanism can work effectively in microscale fluids.

The drag force acting on the outer surface of the tube is negligibly smaller than the reaction force inside it as proved in [11]. That condition sufficiently stands at the swimmer size more than 1 μm assumed in this research.

Therefore, momentum conservation between the tube (with the mass of m and the velocity of v_{eo}) and the inner bulk electrolyte (with the mass of m_f and the velocity of u_{eo}) stands as follows:

$$mv_{eo} + m_f u_{eo} = 0. \tag{1}$$

Their relative velocity is equal to the so-called EOF velocity as follows:

$$u_{eo} - v_{eo} = \frac{\epsilon \zeta}{\eta} \frac{\Delta \phi_{ca}}{L} \tag{2}$$

where L is the body length and $\Delta \phi_{ca}$ is the OCP generated by the BFC (Fig. 1b). ζ is the charged potential of the inner surface of the insulating tube (so-called "zeta potential"). ϵ and η are the permittivity and viscosity of the electrolytic solution.

Self-propulsion velocity model v_{eo} of the tube-shaped swimmer can be derived from Eqs. (1) and (2) as follows: [11]

$$v_{eo} = -\frac{1}{1 + m/m_f} \frac{\epsilon \zeta}{\eta} \frac{\Delta \phi_{ca}}{L},$$

$$\frac{m}{m_f} \simeq \frac{\rho_t}{\rho_f} \cdot \left(\left(\frac{D}{D_t} \right)^2 - 1 \right) \quad (L_e \ll L), \tag{3}$$

where ρ_t and ρ_f are the mass densities of the insulating tube and the electrolyte, respectively, and the total mass of the electrodes is neglected. The diameter ratio D/D_t and the mass ratio m/m_f are assumed to be constant. The OCP $\Delta \phi_{ca}$ does not depend on the electrode size. From Eq. (3), faster v_{eo} is clearly expected by smaller body length L. Therefore, the proposed propulsion mechanism is theoretically suitable and advantageous for use as the self-propulsive microrobot.

10 μm prototype design
The configuration of the new prototype with a size of about 10 μm is shown in Fig. 2a. The two electrodes are made from CPCs incorporating SU-8, conductive NPs such as silver (Ag) or gold (Au) , and anodic or cathodic enzymes with immobilized on the NPs. Other researchers have shown that the SU-8 composite has good electrical conductivity when the volume fraction of the metal NPs for SU-8 solid exceeds about 6 vol% [13]. We used CPC incorporating the enzyme-immobilized AgNPs of 7 vol%. The AgNPs had a mean particle size of 30 nm. An anodic enzyme, such as glucose oxidase (GOx) or glucose dehydrogenase (GDH), are used for one electrode as a bioanode, a cathodic enzyme, such as laccase (LAC) or bilirubin oxidase (BOD), for another electrode as a biocathode. GOx was used as the anodic enzyme and LAC as the cathodic enzyme.
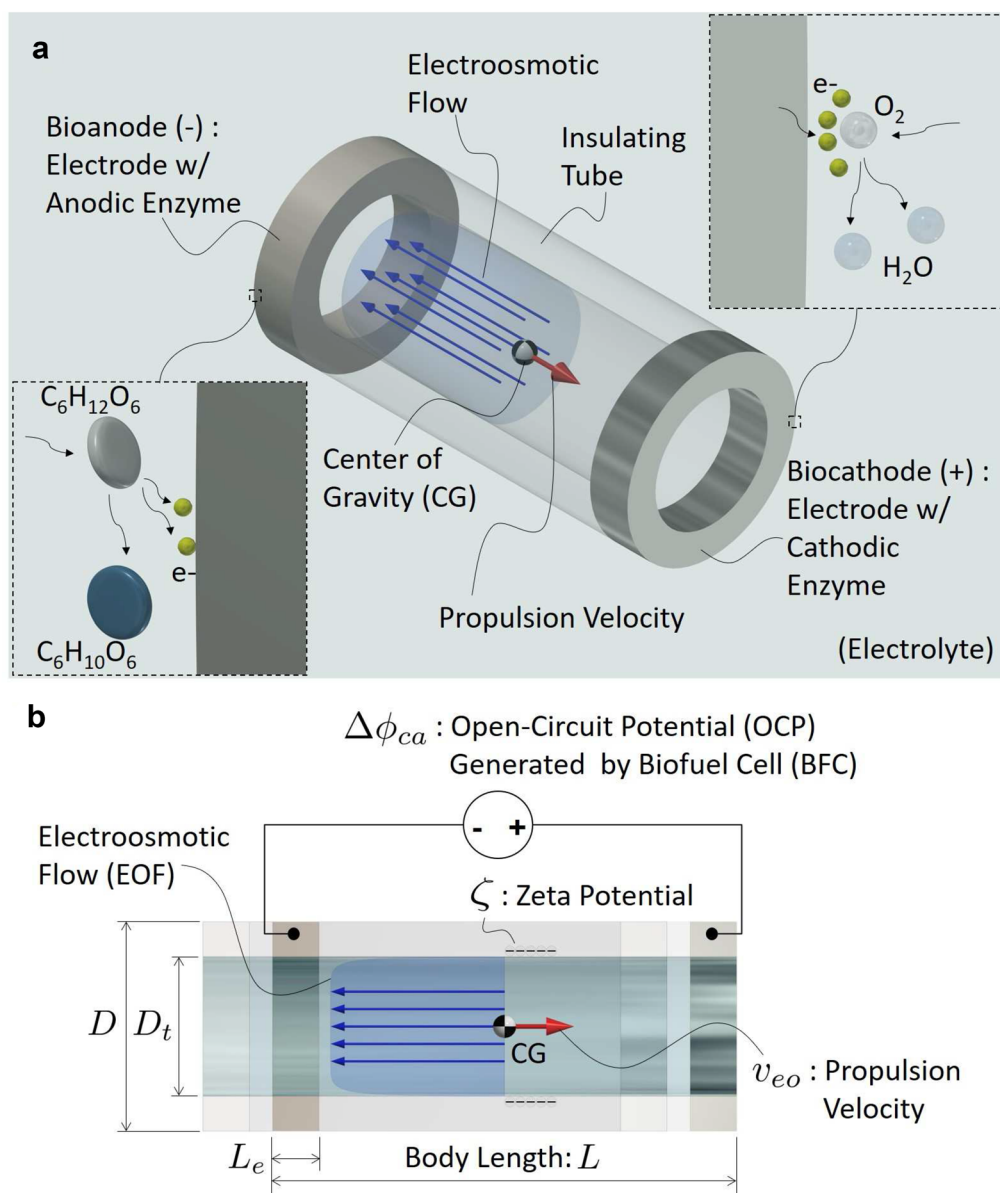
Fig. 1 Concept of microswimmer using BFC and EOP [11]. **a** Configuration and mechanisms. **b** Main parameters

To immobilize the enzymes to AgNPs, we adopted the covalent bonding method using self-assembled monolayers [14] of alkanethiols formed over the NP surfaces like our previous research [11]. The insulating tube is made from NCPC incorporating SU-8 and non-conductive NPs such as fullerene (C_{60}) or magnetite (Fe_3O_4). As a result of several fabrication trials, NCPC was required as the insulating material instead of only SU-8 to use the same power condition of the femtosecond laser for the three layers. The optimal laser power for polymer composites with NPs becomes smaller than that for only polymers because of the radiation

absorption and scattering by the NPs and their agglomerates [15]. We used the NCPC incorporating the fullerene (C_{60}) NPs of 2 vol%. C_{60} NPs were suitable for NCPC because they have good dispersibility in uncured SU-8 fluid.

Fabrication process

The total fabrication process is shown in Fig. 2b. The fabrication process of 10 μm prototypes used femtosecond laser 3D microlithography [12] by "Nanoscribe Photonic Professional" (63×, NA0.75). First, a dextran film as a water-soluble sacrificial layer was patterned on
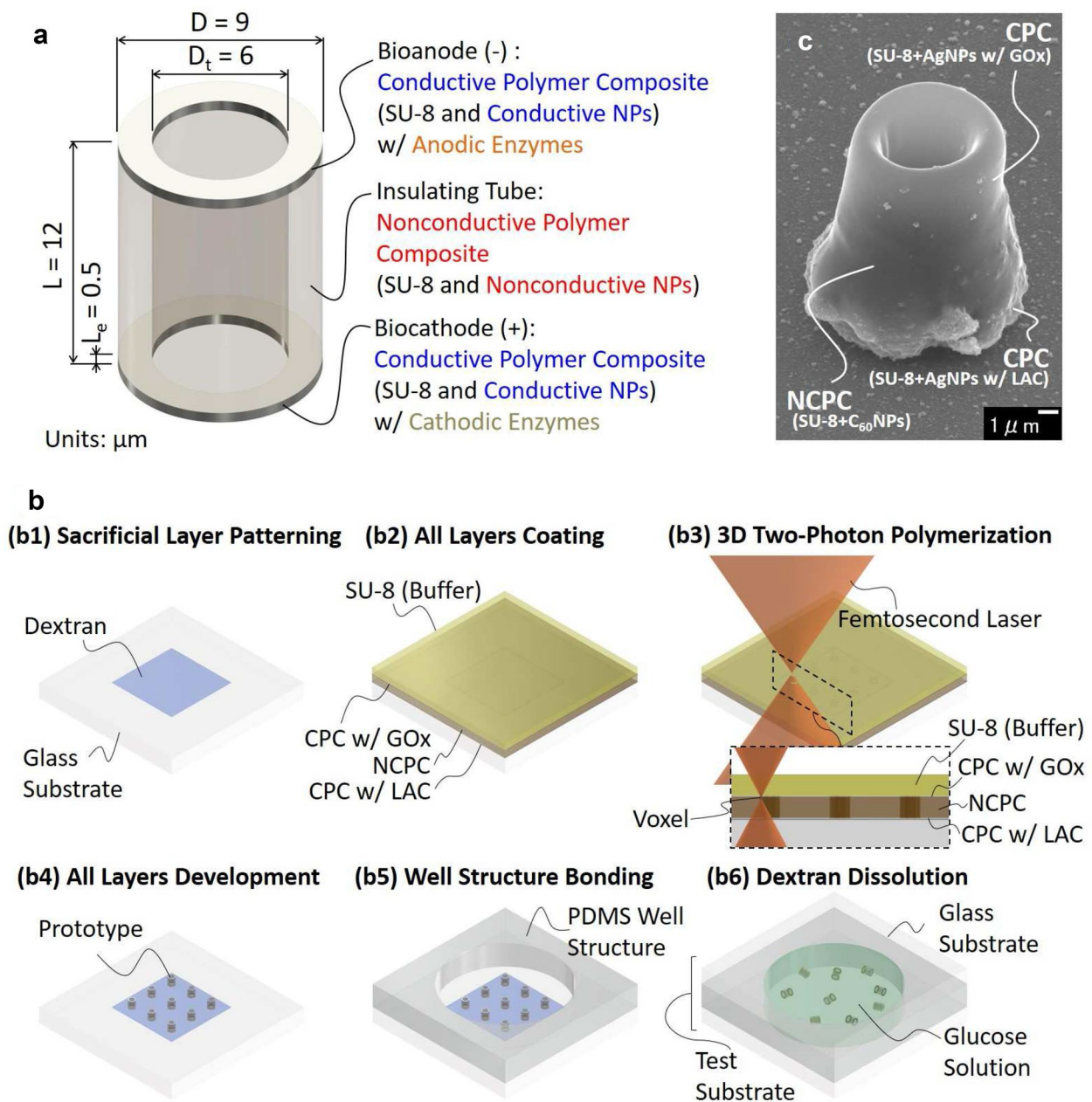
Fig. 2 10 µm prototype. **a** Design and configuration. **b** Fabrication process. **c** Scanning electron microscopic (SEM) images of a fabricated prototype

a glass substrate by the lift-off method [16] as shown in Fig. 2b1. Next, three structural layers (CPC/NCPC/CPC) and an SU-8 buffer layer were coated on the substrate as shown in Fig. 2b2. The buffer layer was required for successful fabrication as described in detail later. To control the thickness of each layer, the viscosity of the material of each layer was adjusted in advance by diluting with cyclopentanone, which is a solvent of uncured SU-8 fluid. A focused spot (so-called "voxel") of the femtosecond laser

(with the wavelength of 780 nm) was scanned in tubelike regions of the structural layers as shown in Fig. 2b3. Only those regions were polymerized due to two-photon absorption.

The optimization trials of fabrication conditions are summarized to Table 1. The optimal laser power was more than 3.0 mW for only SU-8 (Table 1(1)) while it was less than 2.5 mW for only CPC (Table 1(2)). No optimal condition existed between 2.5–6.0 mW for the same

Table 1 The optimization trials of fabrication conditions by using "Nanoscribe Photonic Professional" (63 ×, NA0.75)

Condition	Total thickness (µm)	Laser power (mW)	Scan speed (µm/s)	Result
(1) 1L(SU-8)	0.5–9.0	≥ 3.0	10–30	OK
(2) 1L(CPC)	0.5–1.0	≤ 2.5	10	OK
(3) 3L(CPC/SU-8/CPC)	12.0	2.5–6.0	10	NG
(4) 3L(CPC/NCPC/CPC)	12.0	≤ 2.5	10	NG
(5) 3L(CPC/NCPC/CPC)+buffer(SU-8)	12.0 + 9.0(buffer)	≤ 2.5	10	OK

L: Layer, CPC: SU-8 and AgNPs of 7 vol%, NCPC: SU-8 and C_{60} NPs of 2 vol%

three layers as the previous 100 µm prototype configuration (CPC/SU-8/CPC) (Table 1(3)). The optimal laser power for polymer composites with NPs is assumed to be significantly different from that for only polymers because of the radiation absorption and scattering by the NPs and their agglomerates [15]. Therefore, the same laser power condition is expected for the three structural layers by using NCPC as the material of the insulating layer. However, without the top SU-8 buffer layer, the only lower electrode layer remained (Table 1(4)). The buffer was assumed to be required for the smoothnesses of both optical index and mechanical stress right above the top of the structural three layers. The SU-8 buffer is not polymerized because the laser power 2.5 mW is too small for it. From the above trials, the only successful condition Table 1(5) was derived.

The laser power was set to 2.5 mW and the scan speed 10 µm/s. Finally, through chemical development and cleaning (Fig. 2b4), 10 µm prototypes were successfully fabricated on the substrate as shown in Fig. 2c. During all baking processes, a baking temperature was set to less than 65 °C to avoid deactivation of the enzymes [17]. The thickness of the CPC layer was about 0.5–1.0 µm. The

length of the prototype was about 11.0–20.0 µm depending on the thickness of the NCPC layer.

A test substrate for experiments was fabricated by O_2 plasma bonding of a well structure made of polydimethylpolysiloxane (PDMS) and the glass substrate with the prototypes (Fig. 2b5). A glucose solution (67 mM β-D-glucose, 150 mM NaCl, and fluorescent polystyrene (PS) beads with the size of 3 µm in 10 mM, 7.4 pH phosphate-buffered saline (PBS)) was added in the well. Its glucose concentration was set close to that of the blood of a diabetic patient [1] as the maximum in vivo value. That is the same condition as the previous experiments [11]. The dextran film is water-soluble, so the prototypes were released from the substrate immediately when the solution was added (Fig. 2b6).

Experimental methods

We carried out experiments observing self-propulsions of 10 µm prototypes in a glucose solution using an inverted microscope as shown in Fig. 3. We acquired the videos of the movements from microscopic images, tracked prototypes, and identified propulsion velocities. Finally, we compared those results with the theoretical curves and the results of the previous 100 µm prototypes.
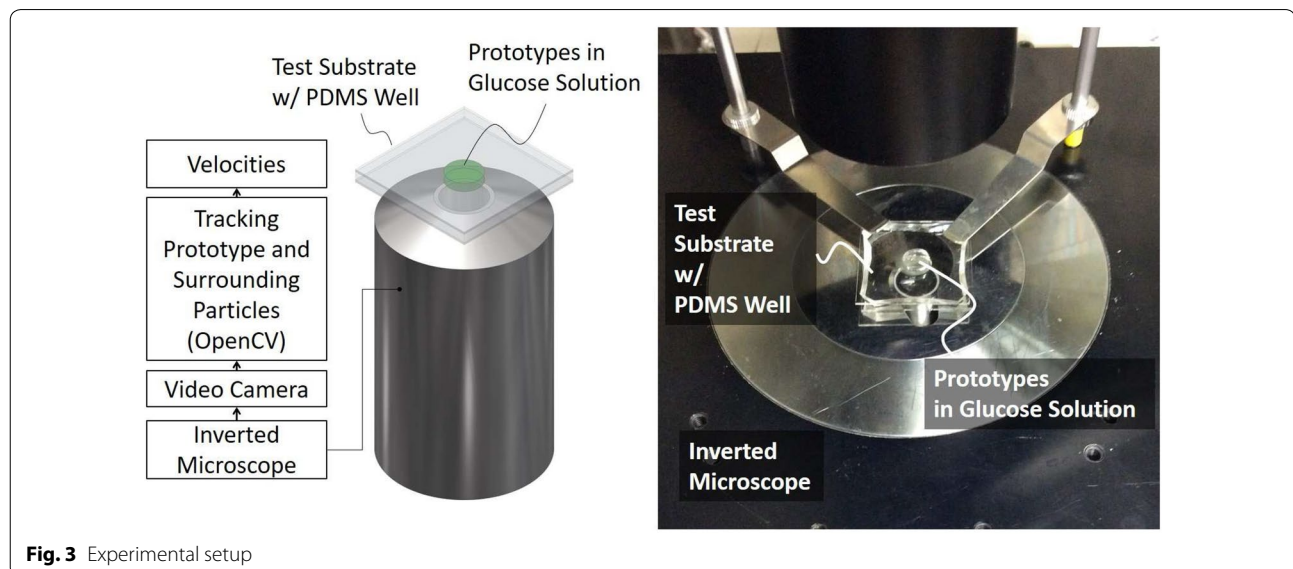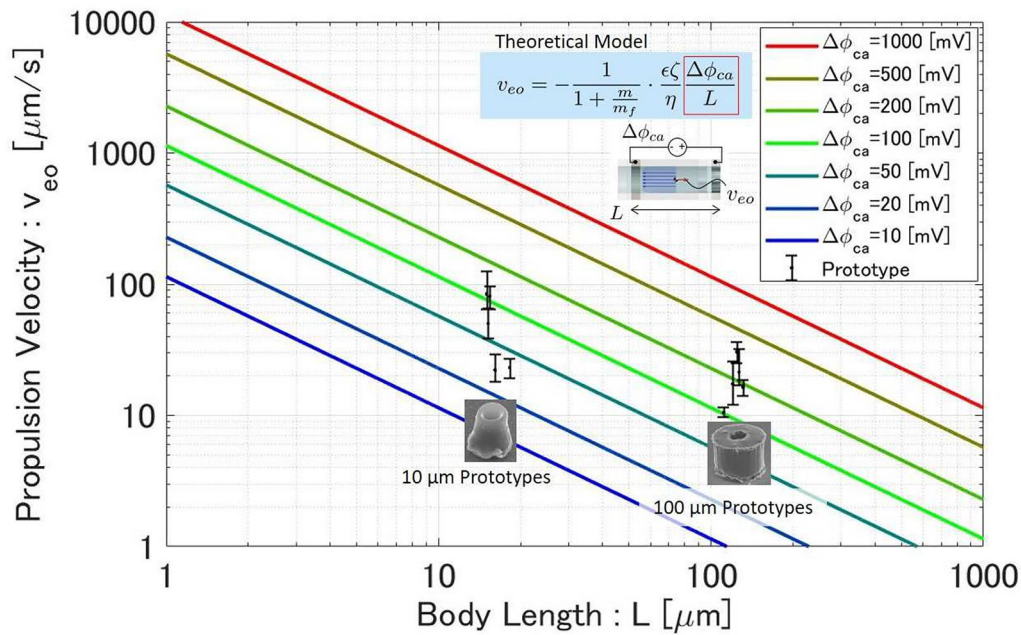

Fig. 3 Experimental setup

Fig. 4 Propulsion velocity against body length: theory and experiments. A point denotes a mean value of v_{eo} experimentally identified and a bar denotes the range. The experimental data of 100 μm prototypes were referenced from [11]

The test substrate was covered with a glass substrate and set on a stage just above the microscope. We can observe and identify unnecessary convective flows by tracking the PS beads in the glucose solution.

After acquiring the video from the microscope, a red circle and a white curve were added to that using "OpenCV" to track the center of gravity (CG) of the prototype and its trajectory. Blue circles with white curves were also added to that by optical-flow processing and they were trajectories of the PS beads or other residues in the surrounding fluid and indicated surrounding convective flows.

The velocities v_p, v_{flow}, and v_{eo} against time t were extracted from the image-processed video with the sampling interval of 0.1 s, where v_p is the velocity of the CG of the prototype, v_{flow} is the mean velocity of the surrounding convective flows in the same direction, and $v_p - v_{flow}$ is identified as the self-propulsion velocity v_{eo}.

Results and discussion

Theoretical performance

Theoretical performance curves were shown in Fig. 4 which were calculated using Eq. (3) with the parameter values from Table 2 and Fig. 1b. From the theoretical curves, faster v_{eo} is clearly expected by smaller body length L. If L can be made smaller than 10 μm, v_{eo} is expected to exceed 1 mm/s, which is close to the blood

Table 2 Parameters [11]

| Meaning	Part	Symbol	Value (units)	Comment
Permittivity	Electrolyte	ϵ	6.580×10^{-10} (F/m)	Water (310 K)
Viscosity	Electrolyte	η	0.692×10^{-3} (Pa s)	Water (310 K)
Mass density	Electrolyte	ρ_f	993 (kg/m^3)	Water (310 K)
Mass density	Insulating tube	ρ_t	1190 (kg/m^3)	SU-8 [18]
Zeta potential	Insulating tube	ζ	-0.030 (V)	SU-8 [19]
OCP	Electrodes	$\Delta\phi_{ca}$	< 1.18 (V)	Theoretical supremum from the Gibbs free energy [20]
Diameter ratio	Swimmer	D/D_t	1.50	
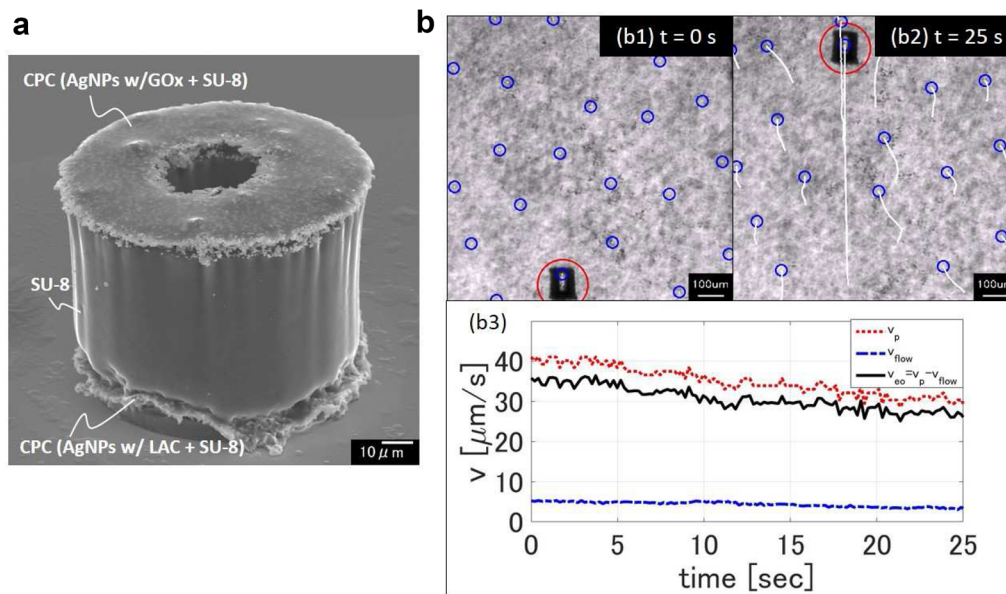
Fig. 5 Results of 100 μm prototypes [11]. **a** SEM image of the 100 μm prototype fabricated by the standard photolithography. **b** Self-propulsion of the fastest 100 μm prototype in a glucose solution. (b1), (b2) Snapshots extracted from a video. A red circle, blue circles, and white curves added by "OpenCV" represent the center of gravity (CG) of the prototype, surrounding particles indicating convective flows, and their trajectories, respectively. (b3) Velocities against time t extracted from the video with the sampling interval of 0.1 s, where v_p is the velocity of the CG of the prototype, v_{flow} the mean velocity of the surrounding convective flows in the same direction, and $v_p - v_{flow}$ the identified self-propulsion velocity v_{eo}
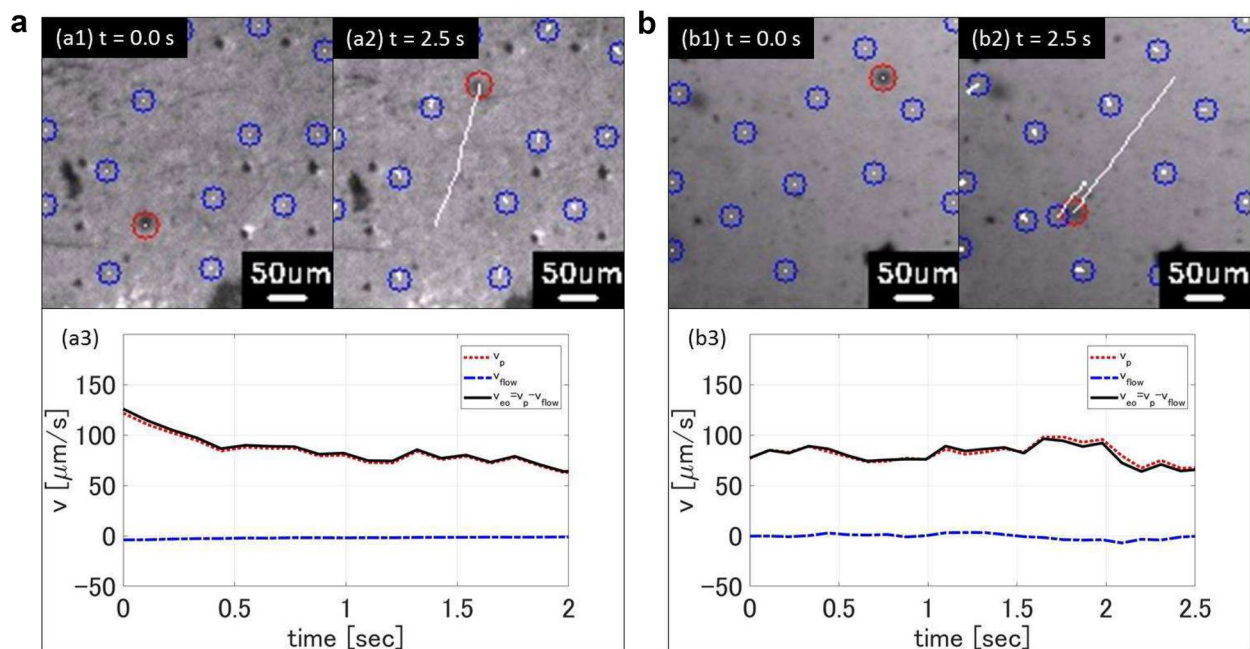

Fig. 6 Self-propulsions of the two fastest 10 μm prototypes in a glucose solution. **a** The fastest prototype. **b** Another prototype. These were processed in the same way as Fig. 5b. Additional files 1 and 2 are the movies of experiments corresponding to **a** and **b**, respectively.

flow in the human capillary system [1]. However, this depends on $\Delta\phi_{ca}$, ζ, and η.

Self-propulsion of previous 100 μm prototypes

In the previous study, we fabricated 100 μm prototypes by the standard photolithography with several alignment and exposure steps as shown in Fig. 5a, and the self-propulsions of them were observed in a glucose solution [11]. Figure 5b shows the fastest results. The trajectory of the CG shows that the movement was in a straight line. Over 25 s, the prototype moved 848 μm. its maximum velocity was identified as 35 μm/s by removing the surrounding convective flow velocities as shown in Fig. 5b3.

Self-propulsion of 10 μm prototypes

Figure 6 shows self-propulsion results of the two fastest 10 μm prototypes. Figure 6a1, a2 show snapshots extracted from the image-processed video. Figure 6a3 shows the velocities v_p, v_{flow}, and v_{eo} against time t extracted from the video. Figure 6b shows another result. The self-propulsions of the 10 μm prototypes were observed (Fig. 6a2, b2). Their trajectories (the white curves with the red circles) show that they moved in the straight lines. There were almost no convective flows (the white curves with the blue circles) around them. Over 2.5 s, the fastest prototype moved 215 μm (Fig. 6a2). A maximum velocity of the prototype was identified as 126 μm/s from Fig. 6a3. A maximum velocity of the fastest 100 μm prototype was 35 μm/s [11]. From the experimental results, the faster velocity by the smaller body size was confirmed as theoretically expected.

Miniaturization effect

Finally, we confirmed the validity of the experimentally identified velocities v_{eo} of the five 10 μm prototypes by comparing with the theory and those of 100 μm prototypes [11] (Fig. 4).

The mean of v_{eo} in the 10 μm prototypes was 100 μm/s and was better than that in the 100 μm prototypes, which was 19 μm/s. However, the range of v_{eo} in the 10 μm prototypes was 18–126 μm/s, while that in the 100 μm prototypes was 10–35 μm/s. The reasons for the large variation in 10 μm prototypes are not exactly clear, but the variation might be due to the diameter ratio D/D_t and the OCP $\Delta\phi_{ca}$ of the prototypes from Eq. (3).

We assume a dimensional error $dD = 1.00$ μm and $(D + dD)/(D_t - dD) = (9.00 + 1.00)/(6.00 - 1.00) = 2.00$ instead of the nominal value $D/D_t = 1.50$. Theoretical v_{eo} with dD is calculated as 54.4 % of its nominal value using Eq. (3). The sensitivity of the D/D_t variation of 10 μm prototypes is relatively large because of its smaller D.

Also the OCP $\Delta\phi_{ca}$ is highly dependent on the activities of the enzymes. Using Eq. (3) with the parameter values from Table 2, the OCPs $\Delta\phi_{ca}$ of the experimental v_{eo} were identified as less than 200 mV and are worse than those of 100 μm prototypes identified as less than 400 mV [11]. The focused spot of femtosecond-laser might have resulted in more inactivation of the enzymes than UV exposure of the standard photolithography.

We consider that resolving this variation issue is one important future work.

Conclusions

We adopted the fabrication method using femtosecond-laser 3D microlithography and multi-materials composing of the conductive polymer composites (CPCs) and nonconductive polymer composite (NCPC) and succeeded in fabricating 10 μm prototypes. Then we demonstrated more than 100 μm/s velocity of the prototype experimentally and proved its validity of the smaller and faster feature. From this experimental verification, this concept is suitable for future biomedical microrobots.

Many challenges still remain for medical applications, such as improving yields, enhancing performance stability, ensuring biocompatibility, and so on. In the next steps, we will develop its strategy to control the microswimmers as microrobots. Also, another embodiments using BFC and EOF mechanisms are biofuel-driven wireless micropumps. They are expected to be applied to perfusions of biological fluids at small local sites inside or outside the human body.

Supplementary information

Supplementary information accompanies this paper at https://doi.org/10.1186/s40648-019-0146-x.

Additional file 1. Movie of experiment corresponding to Fig. 6a.

Additional file 2. Movie of experiment corresponding to Fig. 6b.

Abbreviations

BFC: Biofuel cell; EO: Electroosmotic; EOF: Electroosmotic flow; EOP: Electroosmotic propulsion; OCP: Open-circuit potential; CPC: Conductive polymer composite; NCPC: Nonconductive polymer composite; NP: Nanoparticle; Ag: Silver; C_{60}: fullerene; GOx: Glucose oxidase; LAC: Laccase.

Authors' contributions

TY and FA desinged research. TY performed research. TY analyzed the data. TY and FA wrote the paper. FA provided critical advice on the research strategy and design. Both authors read and approved the final manuscript.

Availability of data and materials

Not applicable.

Ethics approval and consent to participate

Not applicable.

References

1. Freitas RA Jr (1999) Nanomedicine, vol 1. Basic capabilities. Landes Bioscience, Georgetown
2. Chang ST, Paunov VN, Petsev DN, Velev OD (2007) Remotely powered self-propelling particles and micropumps based on miniature diodes. Nat Mater 6(3):235–240
3. Bell DJ, Leutenegger S, Hammar KM, Dong LX, Nelson BJ (2007) Flagella-like propulsion for microrobots using a nanocoil and a rotating electromagnetic field. In: Proceedings of IEEE international conference robotics automation. IEEE, pp. 1128–1133
4. Ghosh A, Fischer P (2009) Controlled propulsion of artificial magnetic nanostructured propellers. Nano Lett 9(6):2243–2245
5. Wu Z, Si T, Gao W, Lin X, Wang J, He Q (2016) Superfast near-infrared light-driven polymer multilayer rockets. Small 12(5):577–582
6. Martel S, Tremblay CC, Ngakeng S, Langlois G (2006) Controlled manipulation and actuation of micro-objects with magnetotactic bacteria. Appl Phys Lett 89(23):233904
7. Sanchez S, Ananth AN, Fomin VM, Viehrig M, Schmidt OG (2011) Superfast motion of catalytic microjet engines at physiological temperature. J Am Chem Soc 133(38):14860–14863
8. Paxton WF, Sen A, Mallouk TE (2005) Motility of catalytic nanoparticles through self-generated forces. Chem Eur J 11(22):6462–6470
9. Mano N, Heller A (2005) Bioelectrochemical propulsion. J Am Chem Soc 127(33):11574–11575
10. Ma X, Jannasch A, Albrecht UR, Hahn K, Miguel-López A, Schäffer E, Sánchez S (2015) Enzyme-powered hollow mesoporous janus nanomotors. Nano Lett 15(10):7043–7050
11. Yamanaka T, Arai F (2018) Self-propelled swimming microrobot using electroosmotic propulsion and biofuel cell. IEEE Robot Autom Lett 3(3):1787–1792
12. Maruo S, Nakamura O, Kawata S (1997) Three-dimensional microfabrication with two-photon-absorbed photopolymerization. Opt Lett 22(2):132–134
13. Jiquet S, Bertsch A, Hofmann H, Renaud P (2005) Conductive SU8 photoresist for microfabrication. Adv Funct Mater 15(9):1511–1516
14. Patel N, Davies MC, Hartshorne M, Heaton RJ, Roberts CJ, Tendler SJ, Williams PM (1997) Immobilization of protein molecules onto homogeneous and mixed carboxylate-terminated self-assembled monolayers. Langmuir 13(24):6485–6490
15. Suter M, Zhang L, Siringil EC, Peters C, Luehmann T, Ergeneman O, Peyer KE, Nelson BJ, Hierold C (2013) Superparamagnetic microrobots: fabrication by two-photon polymerization and biocompatibility. Biomed Microdev 15(6):997–1003
16. Nagai M, Tanizaki K, Kawashima T, Shibata T (2014) Direct assembly of movable parts in a microchannel using a water-soluble sacrificial layer for biohybrid systems. In: 2014 international symposium on micro-nanomechatronics and human science (MHS). IEEE, pp. 1–4
17. Psoma SD, van der Wal PD, Frey O, de Rooij NF, Turner AP (2010) A novel enzyme entrapment in SU-8 microfabricated films for glucose microbiosensors. Biosens Bioelect 26(4):1582–1587
18. Bao XQ, Bontemps A, Grondel S, Cattan E (2011) Design and fabrication of insect-inspired composite wings for mav application using mems technology. J Micromech Microeng 21(12):125020
19. Sikanen T, Tuomikoski S, Ketola RA, Kostiainen R, Franssila S, Kotiaho T (2005) Characterization of SU-8 for electrokinetic microfluidic applications. Lab Chip 5(8):888–896
20. Soukharev V, Mano N, Heller A (2004) A four-electron O_2-electroreduction biocatalyst superior to platinum and a biofuel cell operating at 0.88 V. J Am Chem Soc 126(27):8368–8369

Publisher's Note
Springer Nature remains neutral with regard to jurisdictional claims in published maps and institutional affiliations.